PCCP

PAPER

View Article Online
View Journal | View Issue

Cite this: *Phys. Chem. Chem. Phys.*, 2022, **24**, 9168

Strain modulation in small molecule physisorption in two dimensions: LEED structure analysis and DFT modeling of the system $NaCl(100)/\left(3\sqrt{2}\times\sqrt{2}\right)R45°\text{-}C_2H_2$†

Jochen Vogt

Received 21st December 2021,
Accepted 4th April 2022

DOI: 10.1039/d1cp05827d

rsc.li/pccp

The structure of the system $NaCl(100)/\left(3\sqrt{2}\times\sqrt{2}\right)R45°\text{-}C_2H_2$ was investigated experimentally by means of quantitative LEED *I*(*V*) analysis and computationally using dispersion corrected density functional theory (DFT-D). Three different structure models with four, five, and six molecules were considered. The lowest reliability factors and thus best agreement of measured and calculated *I*(*V*) curves was found for the structure model containing five molecules per surface unit cell. Essential features of the experimental best-fit adlayer structure are supported by DFT. A slight inclination and lateral shift of twofold coordinated molecules away from the on-top position over Na^+ adsorption sites is interpreted as compensation of strain between substrate and adlayer.

1 Introduction

In the absence of covalent bonding between an admolecule and a surface, weak electrostatic forces and dispersive interaction govern the molecule's attachment to the surface and thus its adsorption geometry. Judged on the fairly disentangled electronic structure in such physisorption systems, the latter are occasionally characterized as *simple* systems, although the interplay between molecule–surface and molecule–molecule interaction might lead to a fairly complex growth behaviour, involving order–disorder phase-transitions, and even sequences of several ordered phases. Examples of the latter type are sometimes characterized as (incomplete) devil's staircases.[1,2]

Experimental surface structure analyses on such systems, with the aim to determine the position and orientation of all molecules in the unit cell, however, were restricted so far mostly to systems with compact 2D unit cells with at most two molecules.‡[3–5] Larger unit cells extending over several substrate lattice constants are typically observed if there is a moderate mismatch between the substrate lattice constant and the basal plane lattice parameter of the molecular adsorbate. Acetylene adsorption on the NaCl(100) surface is an example of such a system. The present paper is an attempt to provide the first experimental structure analysis of its $\left(3\sqrt{2}\times\sqrt{2}\right)R45°$ phase and to substantiate a previously suggested structure model involving five translationally inequivalent molecules, thus extending quantitative LEED structure analysis to more complex cases of small molecule physisorption on insulator surfaces.

Adsorption of acetylene on alkali halides has been investigated both experimentally and theoretically in several studies.[4,7–13] On the KCl(100) surface, whose lattice parameter closely matches the intermolecular distance in the basal plane of orthorhombic acetylene,[14] a layer-by-layer growth mode of acetylene thin films was observed in helium atom diffraction experiments.[9] For the first layer, a $\left(\sqrt{2}\times\sqrt{2}\right)R45°$ translational symmetry was deduced,[8] and the adsorbate geometry was completely determined based on quantitative LEED *I*(*V*) structure analysis.[4] On the (100) plane of NaCl, which has a smaller lattice parameter than KCl, the growth of acetylene thin films is more complicated. By means of helium atom scattering (HAS), two different phases were observed,[13] a more dilute phase with $\left(3\sqrt{2}\times\sqrt{2}\right)R45°$ translational symmetry, and a more dense phase with a $\left(7\sqrt{2}\times\sqrt{2}\right)R45°$ unit cell.

While the extremely surface sensitive HAS method is very useful and accurate for the determination of 2D lattice symmetry, the determination of the atomic positions and molecular orientation within the adlayer has not been possible so far. Most promising is LEED *I*(*V*) structure analysis[15,16] for the C_2H_2/NaCl(100) system.

Chemisches Institut der Universität Magdeburg, Universitätsplatz 2, Magdeburg, Germany. E-mail: jochen.vogt@ovgu.de; Fax: +49 391 6711387; Tel: +49 391 6751836

† Dedicated to Prof. Giorgio Benedek on the occasion of his 80th birthday.

‡ An exception is the LEED structure analysis of the system H_2 O-p(3× 2)/MgO(100) with an assumed number of six molecules per unit cell presented in ref. 6. Due to the neglect of hydrogen in electron-scattering, in this case, only oxygen atomic positions and no molecular orientation could be determined.

Low-energy electron diffraction (LEED) is a surface sensitive method, which is well-established for metals and semiconductors. From the analysis of the diffraction peak intensities as a function of electron kinetic energy, a surface structure determination is possible.[15] However, as will become apparent in the rest of this paper, quantitative LEED applied to insulators has to tackle a number of difficulties. From the experimental point of view, surface charging effects are possible when the electron beam strikes the insulator surface.[17] At the same time, surface damage of the very sensitive adsorbate is possible. Both effects are reduced if primary beam currents in the nA range are used and thus the electron exposure is reduced as far as possible. Moreover, the energy window for LEED experiments without extensive charging starts above about 60 eV in the case of NaCl. In this energy range, uncontrollable drifts of the surface potential are suppressed, and the viability of LEED from insulator surfaces has been demonstrated in the literature.[2,3,5,6] However, for a system with a large unit cell and thus many atomic sites that need to be located, the limited energy window starting at above 60 eV reduces the accessible $I(V)$ data range. Especially the fractional order diffraction beams become typically quite weak in intensity at higher energies. The exclusion of the range < 60 eV is thus a serious limitation in this system.

On the other hand, due to the weak molecule–surface interaction, it can be expected that the internal structure of the molecular adsorbate maintains its gas-phase geometry, bond lengths and bond angles are not changed as in the case of chemisorption. This offers the possibility to reduce the number of free parameters in a physically meaningful structure model, and this route is taken in this work.

Quantum chemical studies on the system C_2H_2/NaCl(100) have been reported by Allouche[10] on the Hartree–Fock level. More recently the system has been investigated by Ehrlich *et al.*[11] using various types of dispersion corrected density functional theory (DFT-D2 and DFT-D3) and by Bučko *et al.*[12] using Tatschenko–Scheffler dispersion correction. Both works are focusing on a $(\sqrt{2} \times \sqrt{2})R45°$ unit cell containing two molecules, or on an isolated monomer. A computational study of various unit cell sizes based on the Lennard-Jones model pair potential has been conducted by Picaud *et al.*,[18] including fully fletched phonon calculations.

This paper is organized as follows. In Section 2 the experimental setup is summarized, and experimental data are presented. Moreover, details of the applied LEED $I(V)$ analysis of these data are provided. Structure models are defined and the resulting best-fit geometries are described. Section 3 gives a compact description of the applied DFT methods by means of which minimum energy geometries for the various structure models were obtained. In Section 4 the experimental and computational results are discussed, and potential sources of errors are considered. The paper closes with a short summary.

2 Experimental section

The apparatus for surface science experiments with insulator single crystal surfaces has been described in previous publications.[19,20] The ultrahigh vacuum recipient (base pressure 1×10^{-10} mbar) is equipped with a quadrupole mass spectrometer for gas analysis, and a double microchannelplate LEED optics (Omicron) for diffraction experiments with primary electron currents in the nano-Ampere range to avoid charging of the insulating sample.

A fresh NaCl(100) surface was obtained by cleaving a NaCl single crystal (Korth Kristalle, Germany) in nitrogen atmosphere. For the preparation of the adsorbate layer, the sample was cooled down to a temperature of 75 K. Then the sample was exposed to C_2H_2 (Messer–Griesheim, purity 99.6%) at a partial pressure of 1.0×10^{-8} mbar. Under these conditions, the $(3\sqrt{2} \times \sqrt{2})R45°$ phase grew within four minutes, indicated by the appearance of fractional order diffraction spots. Then the gas exposure was stopped and the sample was cooled down to a temperature of 26 K, resulting in an increase of diffraction peak intensities due to the Debye–Waller effect.[15] LEED patterns (see Fig. 1) were recorded at normal incidence in steps of 2 eV between 70 eV and 300 eV using a CCD camera with 4096 gray values. The operation of the MCPLEED was controlled in such a way that electrons irradiated the surface only during the integration time of the camera, thus reducing electron bombardment of the surface as much as possible. Background corrected integrated beam intensities were generated from the image data using a method described in ref. 21. The resulting set of experimental $I(V)$ curves for seven inequivalent beam orders including three of fractional order is shown in Fig. 2 as thick blue lines. Note that even the brightest fractional order beams are about a factor of 10 lower in intensity.

2.1 LEED $I(V)$ analysis

Due to the multiscattering nature of the interaction of low-energy electrons with matter,[15] the calculation of diffraction beam intensities in LEED is a numerically expensive task which has to be repeated for every electron energy and for every trial geometry considered in a structure analysis. In the present

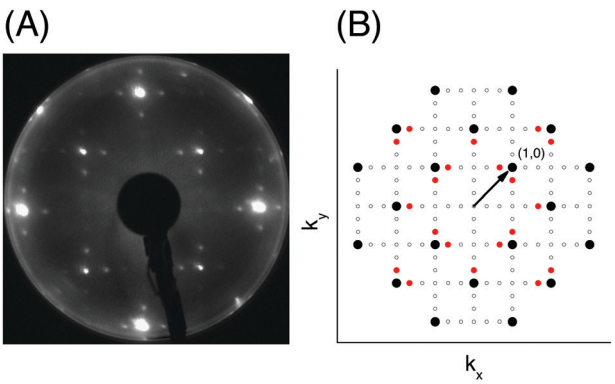

Fig. 1 (A) Diffraction pattern of the acetylene covered NaCl(100) surface, recorded at an electron energy of 120 eV, temperature 75 K. (B) Scheme of reciprocal space of the NaCl(100)/$(3\sqrt{2} \times \sqrt{2})R45°$-$C_2H_2$ surface. Black filled circles mark integral order beam positions, red filled circles indicate additional fractional order spots for which $I(V)$ data are considered. Small open circles mark all other beam-positions.

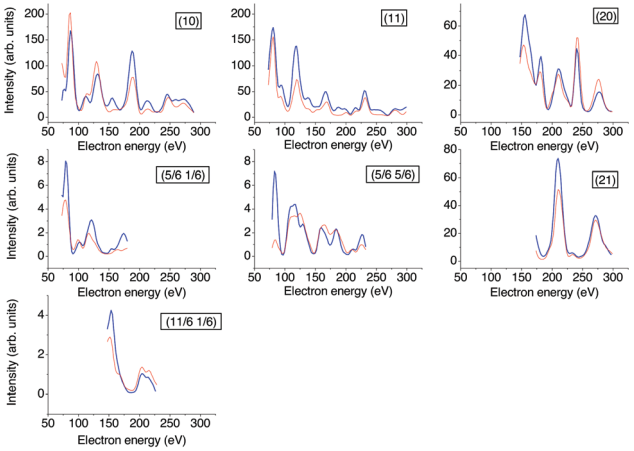

Fig. 2 Experimental *versus* calculated best-fit LEED *I*(*V*) curves. The thicker blue lines represent experimental data recorded at 26 K, the red lines the calculated best-fit spectra for structure model B. For the Pendry *R*-factors see Table 2.

Table 1 Properties of the three classes of structure models investigated with LEED structure analysis. N_t is the number of translationally inequivalent molecules, N_e the number of energetically inequivalent molecules. P is the total number of structure parameters, the sum of P_r substrate rumpling parameters and P_m molecular parameters

Class	N_t	N_e	P_r	P_m	P	Extra symmetry
A	4	2	6	11	17	Glide-plane
B	5	3	8	13	21	2D inversion center
C	6	3	6	16	22	Glide-plane

Table 2 Best-fit overall Pendry *R*-factors and R_P values of beam-orders for the three structure models. Also given is the best-fit real part of the inner potential, V_r

Class	overall R_P	(10)	(11)	(20)	(21)	$(\frac{5}{6}\ \frac{1}{6})$	$(\frac{5}{6}\ \frac{1}{6})$	$\frac{111}{6\ 6}$	V_r (eV)
A	0.22	0.29	0.28	0.19	0.08	0.33	0.28	0.12	−6.3
B	0.14	0.21	0.14	0.08	0.06	0.29	0.10	0.11	−7.0
C	0.20	0.20	0.14	0.13	0.07	0.29	0.42	0.13	−7.0

study, routines of the Barbieri/Van Hove SATLEED package[22] in combination with the Barbieri/Van Hove phase shift package[22] were used to calculate *I*(*V*) spectra. However, the organization of the structure search was controlled by an in-house algorithm. The method minimizes the reliability factor proposed by Pendry,[15,16,23] R_P, by adjusting molecular structure parameters rather than atomic sites, using the gradient-free Powell direction set method.[24] These molecular structure parameters are the Cartesian coordinates of the molecular center of mass, the azimuthal orientation in the crystal frame of reference, and the molecular tilt angle with respect to the surface normal, respectively, as explained below in Section 2.1.1. For the internal structure of the molecules, the gas-phase value of the carbon–carbon bond length of 1.203 Å was assumed.[25] Because of the small electron scattering cross-section of hydrogen,[3,6] only diffraction from carbon atomic sites within the acetylene molecule was considered in the LEED analysis. Phase shifts were considered up to an angular momentum of $l_{max} = 6$. Using $l_{max} = 7$ changed the values of R_P in the best-fit geometry only by about 0.002. Phase shifts were corrected for isotropic thermal vibrations of the scattering sites using fixed root means square (RMS) vibrational amplitudes of 0.11 Å for Cl^-, 0.15 Å for Na^+, and 0.18 Å for carbon. While the NaCl substrate was treated as rigid with a low-temperature bulk lattice constant[26] of 5.60 Å, the vertical positions of the ions in the topmost substrate layer were treated as variable. All beam intensity calculations were carried out in a full dynamic fashion, bypassing the possibility of the very fast tensor LEED approximation,[16] which, however, is only valid if the atomic positions vary no more than about 0.2 Å. Experience with this type of weakly bound adsorbates shows that during a structural search this range is rather often exceeded. The imaginary part of the inner potential was set to a value of $V_i = -3.0$ eV, the real part V_r of the inner potential was automatically adjusted as a non-structural model parameter.

2.1.1 Selection of structure models. In an adsorbate system with several translationally inequivalent weakly interacting molecules, numerous geometries with similar total energy are possible. In order to identify suitable structure models for the NaCl(100)/$(3\sqrt{2} \times \sqrt{2})R45°$-$C_2H_2$ system, it is helpful to consider the geometric arrangement of the molecules in the well-known system KCl(100)/$(\sqrt{2} \times \sqrt{2})R45°$-$C_2H_2$. Here the acetylene molecules are arranged in a checkerboard-like fashion in a T-shaped arrangement of neighboring molecules, which is characteristic for optimized quadrupole–quadrupole interaction of the linear molecules. The molecular axes are strictly parallel to the surface plane, and the low-energy adsorption site is on top of the cation. It is conceivable, that on the NaCl(100) surface a similar structural pattern of T-shaped arrangement is realized. However, due to the lattice mismatch between adsorbate and substrate, the structure may be modulated, including the possibility that strain causes a segmentation of the adsorbate with one or several adsorption sites being vacant. Moreover, it has been observed that in physisorption systems with more than one molecule in the surface unit cell, translationally inequivalent molecules are related by symmetry. Glide-planes are a frequently occurring symmetry element in these systems, and on the KCl(100) surface, the two inequivalent molecules are related by two glide-planes.[4,8] It is conceivable that also in larger unit cells the molecules occupy isoenergetic sites related by symmetry. In the structure models for the acetylene–NaCl(100) system, such extra symmetry is also assumed, which has the effect of a further reduction of independent structure parameters.

Among the possible structure models, three types were preselected based on DFT calculations (see Section 3) and previously published experimental and computational results.[19] These three investigated classes of models are illustrated in Fig. 3, and some properties are summarized in Table 1.

Class *A* (Fig. 5) contains four translationally inequivalent molecules related by glide-plane symmetry along the shorter

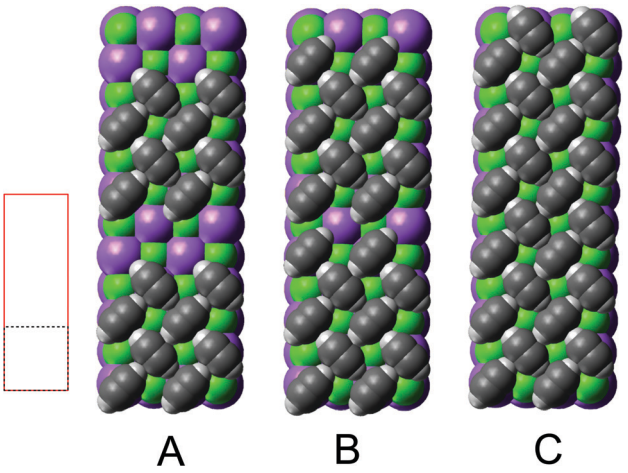

Fig. 3 Structure models A, B, and C for the system $NaCl(100)/(3\sqrt{2}\times\sqrt{2})R45°\text{-}C_2H_2$ with 4, 5, and 6 translationally inequivalent molecules per unit cell, respectively. Shown are 2 × 2 unit cells in top view. The red square rectangle on the left illustrates the extension of the surface unit cell, while the dashed line indicates the reduced size of a $(\sqrt{2}\times\sqrt{2})R45°$ cell. See also Table 1.

side of the unit cell. Thus, the model assumes two energetically inequivalent sites occupied by molecules. The position and orientation of each of these two molecules is described *via* 5 structure parameters, the three cartesian coordinates of the center of mass (COM), and two angles tilt and azimut, as illustrated in Fig. 4. In addition, the distance of the adlayer to the first substrate layer and the rumpling of six inequivalent surface ions gives a total number $P = 17$ structure parameters.

Class *B* (Fig. 6) involves 5 translationally inequivalent molecules related by 2D inversion symmetry in the COM of one molecule, whose lateral position is thus fixed over the cation, and its tilt is parallel to the surface plane by symmetry.

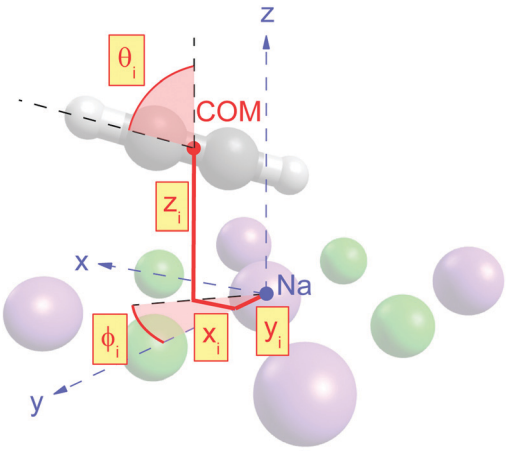

Fig. 4 Illustration of the molecular structure parameters of a molecule M_i adsorbed over a sodium Na. The parameters x_i, y_i, and z_i represent the local position of the center of mass (COM, red point) relative to the sodium (blue point). The azimuthal orientation φ_i is measured against the *y*-axis, the tilt angle θ_i is measured against the surface normal.

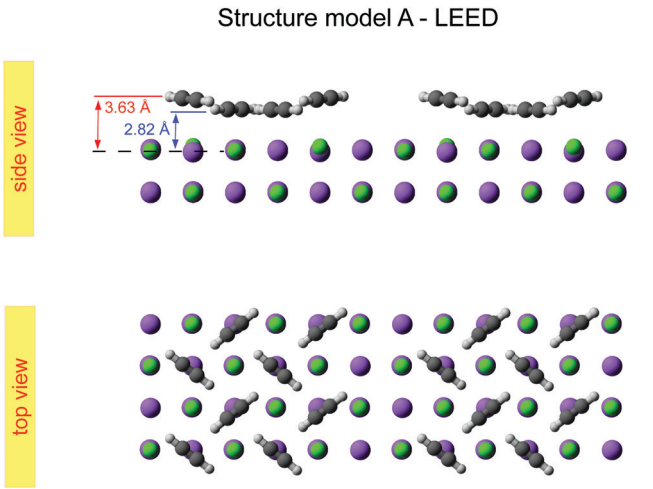

Fig. 5 Best-fit geometry obtained from LEED analysis of structure model A in top view and side view.

Class *C* (Fig. 7), finally, is a full monolayer containing 6 translationally inequivalent molecules, related by glide-plane symmetry. In the absence of any strain modulation, this structure would effectively conform to a $(\sqrt{2}\times\sqrt{2})R45°$ symmetry.

2.1.2 Experimental results. The best-fit geometries in top-view and side-view for the three classes of structure models are shown in Fig. 5, Fig. 6 and Fig. 7. A summary of minimum values of the reliability factors R_P are given in Table 2. Note the general rule, that values of R_P near 0.2 or below are considered to be *good*,[15] which is met by all three structure models. However, the optimization of structure model B with five translationally inequivalent molecules led to a significantly lower value of $R_P = 0.142$, and thus appears to be most reliable. As can be seen in Table 2, the agreement is also acceptable for

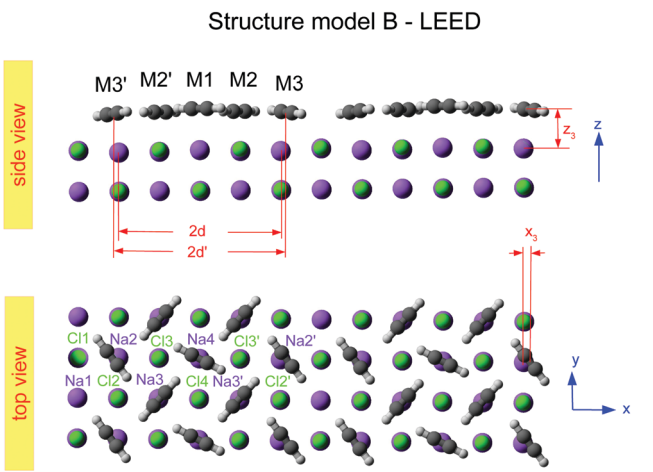

Fig. 6 Best-fit geometry obtained from LEED analysis of structure model B in top view and side view. Structure parameters of the three energetically inequivalent molecules M1, M2, and M3 and vertical shifts of energetically inequivalent ions Na1 to Na4 and Cl1 to Cl4 are given in Table 3. Molecules and ions denoted with a prime are energetically equivalent by symmetry.

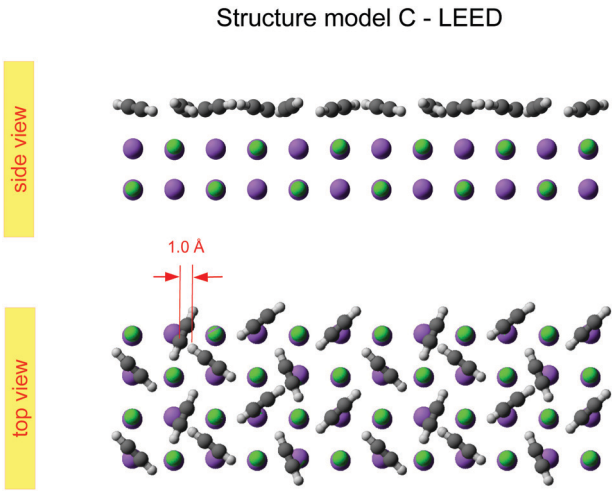

Fig. 7 Best-fit geometry obtained from LEED analysis of structure model C in top view and side view.

all considered beam-orders. For this structure model, the calculated $I(V)$ curves are compared to the experimental data set in Fig. 2. As can be seen in Table 2, the real part of the inner potential measured against zero potential of the vacuum, has a meaningful value of $V_r = -7.0$ eV. A variation of V_r shifts the calculated $I(V)$ spectra in energy, so this this non-structural parameter is automatically adjusted in the structure analysis.

The obtained optimum geometry for structure model A in Fig. 5 with four inequivalent molecules shows the expected nearly T-shaped arrangement of the molecules adsorbed near the cation sites. The vertical distance of the two fourfold coordinated molecules to the surface plane is 2.81 Å. However, the distance of the twofold coordinated molecules is 3.63 Å and thus unrealistically large. Similarly, the optimum geometry for structure model C with six inequivalent molecules in Fig. 7 is characterized by two molecules being unphysically near to each other with some hydrogens approaching the carbon site of the next neighbor molecule as close as 1.0 Å. Apart from the worse agreement judged on their R_P values, some structural features of the obtained geometries of model A and C are thus questionable, leaving model B with also the lowest R_P value as candidate for the real surface structure of the NaCl(100)/$(3\sqrt{2} \times \sqrt{2})R45°$-$C_2H_2$ system. The best-fit parameters of structure model B will be discussed in more detail in the Section 4 in comparison with its minimum energy structure from DFT.

3 DFT calculations

The DFT calculations were performed using the Quantum Espresso package[27–29] (version 6.8). The NaCl(100)/$(3\sqrt{2} \times \sqrt{2})R45°$-$C_2H_2$ surface was represented by a slab of four NaCl layers, separated in vertical direction by 30 Å. A plane wave basis with an energy cutoff of 41 Ry was used in combination with a 2 × 6 × 1 Monkhorst–Pack grid.[30] Projector-augmented wave (PAW) pseudopotentials were taken from A. Dal Corso's library.[31] Geometry optimizations were performed for the structure models A, B, and C (see Fig. 3)

Table 3 Quantities characterizing the best-fit structure from LEED analysis of structure model B, in comparison with results from a DFT-D total energy minimizations. For the position of the molecules M1, M2, and M3, and the ions Na1 to Na4, Cl1 to Cl4, see also Fig. 4. Vertical shifts Δz of substrate ions are taken with respect to the mean z-position of all ions in the first layer. Tilt angles θ of the molecules are measured with respect to the z-axis, azimuthal angles φ are measured against the y-axis, as illustrated in Fig. 4. The positions x, y and z of molecules M1, M2, and M3 are measured against the respective underneath sodium ion position. Values in brackets are estimated errors in units of the last digit

Property	LEED (best-fit)	DFT-D3	DFT-D2
Na1: Δz (Å)	+0.08 (6)	−0.17	−0.15
Cl1: Δz (Å)	+0.08 (4)	−0.05	+0.01
Na2: Δz (Å)	−0.08 (4)	−0.03	−0.01
Cl2: Δz (Å)	−0.08 (4)	+0.03	+0.07
Na3: Δz (Å)	−0.04 (6)	−0.01	−0.00
Cl3: Δz (Å)	+0.07 (4)	+0.08	+0.09
Na4: Δz (Å)	+0.04 (4)	+0.00	+0.00
Cl4: Δz (Å)	−0.04 (4)	+0.08	+0.09
M1: x_1 (Å)	+0 (bysym.)	−0.03	+0.03
M1: y_1 (Å)	+0 (bysym.)	−0.06	−0.06
M1: z_1 (Å)	+2.93 (9)	+2.99	2.76
M1: θ_1 (°)	+90 (bysym.)	+91	+91
M1: φ_1 (°)	−63 (4)	−43	−45
M2: x_2 (Å)	+0.06 (4)	+0.21	+0.13
M2: y_2 (Å)	−0.01 (5)	−0.07	+0.02
M2: z_2 (Å)	2.73 (9)	+2.98	3.11
M2: θ_2 (°)	+90 (3)	+92	+89
M2: φ_2 (°)	+42 (3)	+44	+44
M3: x_3 (Å)	+0.43 (5)	+0.49	+0.34
M3: y_3 (Å)	−0.02 (3)	−0.17	−0.02
M3: z_3 (Å)	+2.62 (9)	+2.98	2.77
M3: θ_3 (°)	+95 (2)	+94	+94
M3: φ_3 (°)	−38 (2)	−48	−45

using Perdew–Burke–Ernzerhof (PBE) functionals augmented with Grimme's DFT-D2 correction[32] for dispersive interaction, as well as the DFT-D3 correction.[33] Apart from translational symmetry, no extra symmetry was used. Vertical positions of the ions in the bottom layer were fixed to the unrelaxed bulk position with a lattice constant of 5.70 Å, the latter being preoptimized in variable-cell relaxation of bulk NaCl. For a given structure with n molecules, the adsorption energy E_c per molecule at 0 K was calculated from

$$E_{ad} = \frac{1}{n}[E(C_2H_2, NaCl) - nE(C_2H_2) - E(NaCl)] + \Delta E_{ZPE} \quad (1)$$

with E (C_2H_2,NaCl), E (C_2H_2), and E (NaCl) being the total DFT-D energies of the considered structure, an isolated acetylene molecule, and a bare relaxed NaCl surface slab, respectively. ΔE_{ZPE} is the simplest approximation to the change of zero-point-energy (ZPE) per molecule. For a physisorption system of n molecules and n_{subs} atoms of the bare substrate, the change of total ZPE is[34]

$$\Delta E_0 \approx \frac{\hbar}{2}\left(\sum_i^n \omega_i^{phys} - \sum_i^{n_{subs}} \omega_i^{subs} - \sum_i^n \omega_i^{gas}\right) \quad (2)$$

Here, ω_i^{phys} are the phonon frequencies of the physisorbate at the Γ-point, ω_i^{subs} the respective frequencies of the bare substrate, and ω_i^{gas} the frequencies of the isolated molecule in the gas-phase. The weak molecule–surface interaction leaves the *inner* modes of the molecule and the substrate modes essentially unchanged. It can thus be expected that the main contribution to ΔE_0 is from the

external vibrational modes[34,35] of the adsorbed molecules (five per molecule). Dunn and Ewing[36] estimated the average frequency of these external modes to be $\omega^{av} = 100\ cm^{-1}$, which is roughly in agreement with results of phonon calculations by Picaud *et al.*,[18] according to which the mostly dispersionless phonon modes assigned to the admolecules lie between 4 and 23 meV, in average 13.5 meV. Thus, the simplest estimate to the zero point energy contribution per molecule is

$$\Delta E_{ZPE} \approx 5\frac{\hbar\omega^{av}}{2} \approx 3.0\ kJ\ mol^{-1}, \quad (3)$$

and this value shall be used for all structure models.

3.1 DFT results

Total energy minimization of the structures shown in Fig. 3 did, as expected, not significantly change the internal structure of the adsorbed molecules. The DFT-D3 optimization led to carbon–carbon bond lengths of $r_{CC} = 1.211$ Å and carbon–hydrogen bond lengths of $r_{CH} = 1.075$ Å, in both cases slightly overestimating the respective experimental gas-phase values[25] of 1.203 Å and 1.062 Å, respectively. DFT-D2 optimizations led to $r_{CC} = 1.211$ Å and $r_{CH} = 1.076$ Å. A similar trend of bond length overestimation of these methods was previously observed for carbon dioxide.[37] The adsorption energies of the various structures after optimization are presented in Table 4. For both versions of dispersion correction, the full monolayer structure C with 6 molecules per unit cell is lowest in energy. However, in optimizations with DFT-D3, structure B with five molecules is only slightly higher in energy by about 0.1 kJ mol^{-1}, while in optimizations with DFT-D2 this difference is 1.4 kJ mol^{-1} and thus considerably larger. The PBE/DFT-D3 adsorption energies are closer to the experimental value[36] of the isosteric heat of adsorption of 30 kJ mol^{-1} at $T \sim 80$ K. Note that the calculated adsorption energies at zero Kelvin are not sufficient to predict the stability of the considered geometries at a finite temperature, and that a full stability analysis based on Gibbs free adsorption energies[34] is beyond the scope of this paper.

4 Discussion

The presented results of the LEED structure analysis support model B with five translationally inequivalent molecules per unit cell. Additional support of this structure model can be gained from comparing the best-fit geometry with the minimum energy structures obtained from DFT. Table 3 summarizes and compares sets of structure parameters. For the eight energetically inequivalent ion positions of the topmost substrate layer, their vertical displacements relative to their geometrical mean vertical position are given as parameter Δz. These ionic sites are indicated in Fig. 6 as Na i, and Cl i, $i = 1,\ldots,4$. Molecular parameters for the three inequivalent molecules Mi, $i = 1,\ldots,3$, are the position x_i, y_i, and z_i measured with respect to the position of the local sodium ion, over which the molecule is situated. The orientation of the molecules is characterized by means of the azimuthal angle φ_i measured against the y-axis, and the tilt θ_i with respect to the surface normal, respectively. Comparison of the geometries depicted in Fig. 6 and Fig. 8 reveals several common features. Firstly, from the top view perspective, the nearly T-shaped arrangement of neighboring molecules is evident. However, according to LEED, the azimuthal angles vary more strongly between $-63°$ for the fourfold coordinated molecule M1, $+42°$ for molecule M2, and $-38°$ for the twofold coordinated molecule M3, indicating more flexibility in the lateral orientation than predicted by DFT, for which both versions of DFT-D give values near to $\pm 45°$. A lateral layer expansion in the sense that the mean distance $2d'$ (see Fig. 6) between the acetylene molecules M3 and M3′ in x-direction is larger than twice the substrate lattice parameter $2d$ can be deduced both from LEED and DFT. Both methods find a lateral shift of the molecule M3 in x-direction of $x_3 \sim 0.4$ Å. Thus, based on the parameter set obtained by LEED, the resulting parameter $2d' = 2(d + x_3)$ is consistent with $d' = 6.0(1)$ Å. This value is close to the solid-state acetylene lattice parameter $a_0 = 6.09$ Å in its orthorhombic phase.[14] A possible interpretation of this lateral adlayer expansion is based on strain in a system with lattice misfit: a strict on top adsorption of acetylene would lead to a compressed surface layer with increased intermolecular repulsion. The twofold-coordinated molecules M3 and M3′ compensate this resulting strain by a slight lateral shift. Interestingly, DFT-D predicts also a weaker shift of molecules M2 and M2′ in the order of 0.1 to 0.2 Å depending on the version of dispersion correction, while the result based on LEED structure analysis is consistent with a weaker displacement in x-direction of 0.06 ± 0.04 Å. Moreover, according to

Table 4 Adsorption energies at $T = 0$ K of optimized structures, see Fig. 3. All values are given in kJ mol^{-1}. The values in brackets are the respective values without ZPE correction

Model	E_{ad} (PBE/DFT-D3)	E_{ad} (PBE/DFT-D2)
A	−30.7 (−33.7)	−36.3 (−39.3)
B	−31.6 (−34.6)	−36.9 (−39.9)
C	−31.7 (−34.7)	−38.3 (−41.3)
Exp[a]	−30 (2) at $T \sim 80$ K	

[a] The experimental value by Dunn and Ewing[36] corresponds to the isosteric heat of adsorption at temperatures near 80 K.

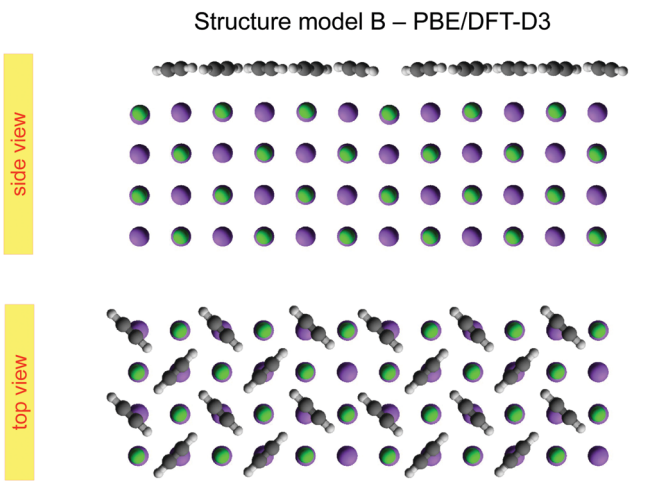

Fig. 8 Minimum energy structure for model B, calculated from a PBE/DFT-D3 geometry optimization of a four layer slab.

LEED, the twofold coordinated molecules M3 are somewhat inclined with $\theta_3 = 95 \pm 2^\circ$, also in accordance to the value of 94° predicted by both versions of DFT-D. Again, this inclination towards the substrate could be interpreted as stabilization of the only twofold coordinated molecules due to increased molecule–substrate interaction. The structure supported by LEED in Fig. 6 inspected from side view reveals a curved variation of the vertical distance of the molecules (Fig. 6), with molecule M3 being closest to the surface plane, and M1 at 2.93 ± 0.09 Å above the Na^+ cation underneath. An explanation of this modulation of vertical distances may be based on strain. However, this structural feature is not supported by DFT-D3, which predicts very similar values for the parameters z_i, i = 1,...,3 of 2.99 to 2.98 Å.

These aforementioned structural similarities are a strong basis for the validity of structure model B. A look on the vertical shifts of the ions in the first layer, however, reveals also differences, which need to be discussed. The most obvious difference is the position of ion Na1, *i.e.* the sodium site which is not occupied by an acetylene molecule. The LEED analysis suggests an elevated position of Na1 and Cl1 of +0.08 Å over the surface plane, while both DFT-D methods predict an unusually large inward shift of the sodium ion Na1 of −0.17 Å (DFT-D3) and −0.15 Å (DFT-D2), respectively. The relaxation of ions at the NaCl surface is driven by comparatively small energy differences of less than 1 kJ mol^{-1} per substrate surface unit cell. It is thus conceivable that relaxation patterns with slightly higher energy exist, that could become more favorable if other functionals and dispersion correction are used. From the experimental point of view, some limitations of the LEED analysis method especially for insulator surfaces have been mentioned above in Section 1. As the shape of the potential energy surface may be influenced by the choice of functionals in DFT, the profile of reliability factors in LEED may be influenced by the choice of non-structural parameters, phase shifts and vibrational amplitudes. These non-structural parameters used in the present study were chosen based on the experience obtained in previous work.[4,38,39] Vibrational amplitudes in general do not strongly alter the R_P values.[15] Thus, as is common practice, fixed RMS were assigned to the various chemical elements. Strictly speaking, however, the site Na1 could be considered as vibrationally inequivalent from the other sites, since it is not occupied by an admolecule. The use of a different vibrational amplitude for this ion could thus be a way of further refinement of the model. Moreover, a further systematic error in LEED analysis might result from the use of isotropic vibrational amplitudes for the ionic sites. While the correction of phase shifts for *anisotropic* displacements of ions is possible,[40] such a refinement of the method would also drastically increase the number of parameters in the structure analysis – contrary to the intention of the present work, which was to maintain structure models with a minimum number of parameters. Such refinements could be envisaged in future experimental work.

5 Conclusions

Weakly bound adsorbates on insulating substrates may show complex surface geometries in two dimensions. The application of low-energy electron diffraction to these systems is a route to gain insight into their structure, if extensive surface charging may be avoided, and if suitable structure models can be developed based on previous experimental work and theoretical considerations. In the present work, the structure of the system NaCl(100)/$(3\sqrt{2} \times \sqrt{2})R45°$-$C_2H_2$ was investigated experimentally by means of quantitative LEED analysis using three classes of structure models with four, five, and six molecules, respectively. Best agreement was found for a structure of five molecules per unit cell in an T-shaped arrangement of nearly flatly adsorbed molecules over sodium sites. In agreement with dispersion corrected DFT total energy minimizations, a lateral adlayer expansion along the longer axis of the unit cell was found and interpreted by strain due to the lattice misfit between the NaCl substrate surface and the acetylene adlayer.

Conflicts of interest

There are no conflicts to declare.

Acknowledgements

I am grateful to the University of Magdeburg and its facilities for financial and technical support of the ongoing projects.

Notes and references

1 P. Bak, *Rep. Prog. Phys.*, 1982, **45**, 587–629.
2 P. Audibert, M. Sidoumou and J. Suzanne, *Surf. Sci.*, 1992, **273**, L467–L471.
3 D. Ferry, P. N. M. Hoang, J. Suzanne, J.-P. Bibérian and M. A. Van Hove, *Phys. Rev. Lett.*, 1997, **78**, 4237–4240.
4 J. Vogt and H. Weiss, *Phys. Rev. B: Condens. Matter Mater. Phys.*, 2008, **77**, 125415.
5 J. Vogt and H. Weiss, *J. Chem. Phys.*, 2003, **119**, 1105–1114.
6 D. Ferry, S. Picaud, P. Hoang, C. Girardet, L. Giordano, B. Demirdjian and J. Suzanne, *Surf. Sci.*, 1998, **409**, 101–116.
7 A. Allouche, *J. Phys. Chem.*, 1996, **100**, 17915–17922.
8 A. L. Glebov, V. Panella, J. P. Toennies, F. Traeger, H. Weiss, S. Picaud, P. N. M. Hoang and C. Girardet, *Phys. Rev. B: Condens. Matter Mater. Phys.*, 2000, **61**, 14028–14036.
9 J. P. Toennies, F. Traeger, H. Weiss, S. Picaud and P. N. M. Hoang, *Phys. Rev. B: Condens. Matter Mater. Phys.*, 2002, **65**, 165427.
10 A. Allouche, *Surf. Sci.*, 1997, **374**, 117–124.
11 S. Ehrlich, J. Moellmann, W. Reckien, T. Bredow and S. Grimme, *ChemPhysChem*, 2011, **12**, 3414–3420.
12 T. Bučko, S. Lebegue, J. G. Angyan and J. Hafner, *J. Chem. Phys.*, 2014, **141**, 034114.
13 A. Glebov, R. E. Miller and J. P. Toennies, *J. Chem. Phys.*, 1997, **106**, 6499–6506.
14 R. K. McMullan, Å. Kvick and P. Popelier, *Acta Crystallogr., Sect. B: Struct. Sci.*, 1992, **48**, 726–731.
15 M. A. Van Hove, W. H. Weinberg and C.-M. Chan, *Low-Energy Electron Diffraction*, Springer, Berlin, 1986.

16 M. Van Hove, W. Moritz, H. Over, P. Rous, A. Wander, A. Barbieri, N. Materer, U. Starke and G. Somorjai, *Surf. Sci. Rep.*, 1993, **19**, 191–229.
17 J. Cazaux, *J. Electron Spectrosc. Relat. Phenom.*, 2010, **176**, 58–79.
18 S. Picaud, P. N. M. Hoang, C. Girardet, A. Glebov, R. E. Miller and J. P. Toennies, *Phys. Rev. B: Condens. Matter Mater. Phys.*, 1998, **57**, 10090–10099.
19 A. G. Cabello-Cartagena, J. Vogt and H. Weiss, *J. Chem. Phys.*, 2010, **132**, 074706.
20 J. Vogt, in *Encyclopedia of Interfacial Chemistry*, ed. K. Wandelt, Elsevier, Oxford, 2018, pp. 202–212.
21 G. Held, S. Uremovic, C. Stellwag and D. Menzel, *Rev. Sci. Instrum.*, 1996, **67**, 378–383.
22 A. Barbieri and M. A. Van Hove, *Barbieri/Van Hove SATLEED package*, available from M. A. Van Hove.
23 J. B. Pendry, *J. Phys. C: Solid State Phys.*, 1980, **13**, 937–944.
24 W. Press, B. Flannery, S. Teukolsky and W. Vetterling, *Numerical Recipes in FORTRAN 77: The Art of Scientific Computing*, Cambridge University press, Cambridge, 1992.
25 H. Edwards, *Spectrochim. Acta, Part A*, 1990, **46**, 97–106.
26 W. Pies and A. Weiss, *Landolt-Börnstein Vol. III/7a: Crystal Structure Data of Inorganic Compounds: Halides and Complex Halides*, Springer, 1973.
27 P. Giannozzi, O. Baseggio, P. Bonfà, D. Brunato, R. Car, I. Carnimeo, C. Cavazzoni, S. de Gironcoli, P. Delugas, F. Ferrari Ruffino, A. Ferretti, N. Marzari, I. Timrov, A. Urru and S. Baroni, *J. Chem. Phys.*, 2020, **152**, 154105.
28 P. Giannozzi, O. Andreussi, T. Brumme, O. Bunau, M. B. Nardelli, M. Calandra, R. Car, C. Cavazzoni, D. Ceresoli, M. Cococcioni, N. Colonna, I. Carnimeo, A. D. Corso, S. de Gironcoli, P. Delugas, R. A. DiStasio, A. Ferretti, A. Floris, G. Fratesi, G. Fugallo, R. Gebauer, U. Gerstmann, F. Giustino, T. Gorni, J. Jia, M. Kawamura, H.-Y. Ko, A. Kokalj, E. Küçükbenli, M. Lazzeri, M. Marsili, N. Marzari, F. Mauri, N. L. Nguyen, H.-V. Nguyen, A. O. de-la Roza, L. Paulatto, S. Poncé, D. Rocca, R. Sabatini, B. Santra, M. Schlipf, A. P. Seitsonen, A. Smogunov, I. Timrov, T. Thonhauser, P. Umari, N. Vast, X. Wu and S. Baroni, *J. Phys.: Condens. Matter*, 2017, **29**, 465901.
29 P. Giannozzi, S. Baroni, N. Bonini, M. Calandra, R. Car, C. Cavazzoni, D. Ceresoli, G. L. Chiarotti, M. Cococcioni, I. Dabo, A. D. Corso, S. de Gironcoli, S. Fabris, G. Fratesi, R. Gebauer, U. Gerstmann, C. Gougoussis, A. Kokalj, M. Lazzeri, L. Martin-Samos, N. Marzari, F. Mauri, R. Mazzarello, S. Paolini, A. Pasquarello, L. Paulatto, C. Sbraccia, S. Scandolo, G. Sclauzero, A. P. Seitsonen, A. Smogunov, P. Umari and R. M. Wentzcovitch, *J. Phys.: Condens. Matter*, 2009, **21**, 395502.
30 H. J. Monkhorst and J. D. Pack, *Phys. Rev. B: Condens. Matter Mater. Phys.*, 1976, **13**, 5188–5192.
31 A. Dal Corso, *Comput. Mater. Sci.*, 2014, **95**, 337–350.
32 S. Grimme, *J. Comput. Chem.*, 2006, **27**, 1787–1799.
33 S. Grimme, J. Antony, S. Ehrlich and H. Krieg, *J. Chem. Phys.*, 2010, **132**, 154104.
34 D. Loffreda, *Surf. Sci.*, 2006, **600**, 2103–2112.
35 A. Lakhlifi and C. Girardet, *Surf. Sci.*, 1991, **241**, 400–415.
36 S. K. Dunn and G. E. Ewing, *J. Phys. Chem.*, 1992, **96**, 5284–5290.
37 M. K. Rana, H. S. Koh, J. Hwang and D. J. Siegel, *J. Phys. Chem. C*, 2012, **116**, 16957–16968.
38 J. Vogt, *Phys. Rev. B: Condens. Matter Mater. Phys.*, 2007, **75**, 125423.
39 J. Vogt and B. Vogt, *J. Chem. Phys.*, 2014, **141**, 214708.
40 V. Fritzsche, *Phys. Rev. B: Condens. Matter Mater. Phys.*, 1994, **50**, 1922–1928.